Journal of Neuroscience Methods 195 (2011) 222–231

Contents lists available at ScienceDirect

Journal of Neuroscience Methods

journal homepage: www.elsevier.com/locate/jneumeth

Automated and quantitative image analysis of ischemic dendritic blebbing using *in vivo* 2-photon microscopy data

Shangbin Chen, Sherri Tran, Albrecht Sigler, Timothy H. Murphy*

Department of Psychiatry, Brain Research Centre, University of British Columbia, Vancouver, BC, Canada, V6T 1Z3

ARTICLE INFO

Article history:
Received 12 October 2010
Received in revised form
11 December 2010
Accepted 13 December 2010

Keywords:
Automated approach
Dendritic blebbing
Adaptive thresholding
Ischemia
Two-photon imaging

ABSTRACT

Ischemia induces a 'blebbing' of dendrites, a structural alteration where dendrites take on a 'beads on a string' appearance. We developed a toolkit program, *BlebQuant*, for quantitative automated bleb analysis to chart the morphology of dendrites labeled with GFP/YFP under normal conditions and after ischemia-induced damage. *In vivo* 2-photon data from mouse layer 5 neurons with apical dendritic tufts extending to the cortical surface were examined before, during, and after global ischemia. To quantify changes in dendritic structure, we used morphometric tools that exploit characteristic features of blebbing, distinguished as localized regions of spherical or ellipsoid swellings. By comparing acquired images during ischemia and reperfusion to a pre-ischemia reference image, our automated approach detected blebs based on defined eccentricity and area thresholds and quantified the percentage of blebbed dendrites based on a block-selection method. Our results indicate that the automated morphometric indices we employ yield results that correlate with manual assessment. The automated approach permits rapid and effective analysis of dendritic structure and may facilitate the study of ischemic dendritic damage.

1. Introduction

Transgenic mice expressing fluorescent proteins have recently become a tool to examine real time changes in synapses and dendrites in models of stroke and neurodegenerative disease (Davalos et al., 2005; Feng et al., 2000; Spires et al., 2005). In particular, studies have investigated alterations of dendritic spines in stroke (Brown et al., 2007, 2008; Brown and Murphy, 2008; Mostany et al., 2010; Risher et al., 2010). In addition to changes to spines, under certain conditions, the dendritic branch can also be structurally dynamic. During ischemia, dendrites take on a distinct pattern of structural damage termed 'blebbing'. Blebbing is characterized as localized regions of spherical or ellipsoid ('varicose') swellings, resembling a 'beads on a string' appearance (Hasbani et al., 2001; Li and Murphy, 2008; Murphy et al., 2008; Obeidat et al., 2000; Park et al., 1996; Zhang et al., 2005; Zhang and Murphy, 2007).

We have previously reported the rapid induction of blebbing within minutes of both focal and global models of stroke in apical dendrites of layer 5 neurons using *in vivo* 2-photon (2P) imaging (Li and Murphy, 2008; Murphy et al., 2008; Zhang and Murphy, 2007). Interestingly, this structural damage may not always be permanent as dendrites show a certain degree of recovery with reperfusion (Murphy et al., 2008), and those within a penumbra are able to recover between periods of spontaneous peri-infarct spreading depolarization (Risher et al., 2010).

While there has been much work describing dendritic blebbing, to this date, procedures for the identification and quantification of blebs have relied on a manual approach which is labor intensive and can be subjective. In this paper, we describe our approaches in developing *BlebQuant*, a toolkit program which allows automated examination of changes in dendritic structure induced by ischemia in mouse somatosensory cortex *in vivo* (Li and Murphy, 2008; Murphy et al., 2008; Zhang et al., 2005; Zhang and Murphy, 2007). Our approach relies on exploiting morphological features of blebs such as eccentricity and changes in area of blebbed regions. Fig. 1 summarizes our MATLAB-based approach (MATLAB R2008a, the MathWorks, Natick, MA) for the detection and quantification of blebs. We report that this approach provides a quantitative unbiased appraisal of ischemic damage that is comparable with blinded manual analysis.

2. Materials and methods

2.1. Image acquisition

Male C57BL6 (2–5 months of age) yellow fluorescent protein (YFP) and green fluorescent protein (GFP) expressing transgenic mice (H and M lines) (Feng et al., 2000) were used in this

* Corresponding author at: Department of Psychiatry, Brain Research Centre, 4N1-2255, Wesbrook Mall, University of British Columbia, Vancouver, BC, Canada, V6T 1Z3. Tel.: +1 604 822 0705; fax: +1 604 822 7981.
E-mail address: thmurphy@interchange.ubc.ca (T.H. Murphy).

0165-0270/$ – see front matter.
doi:10.1016/j.jneumeth.2010.12.018

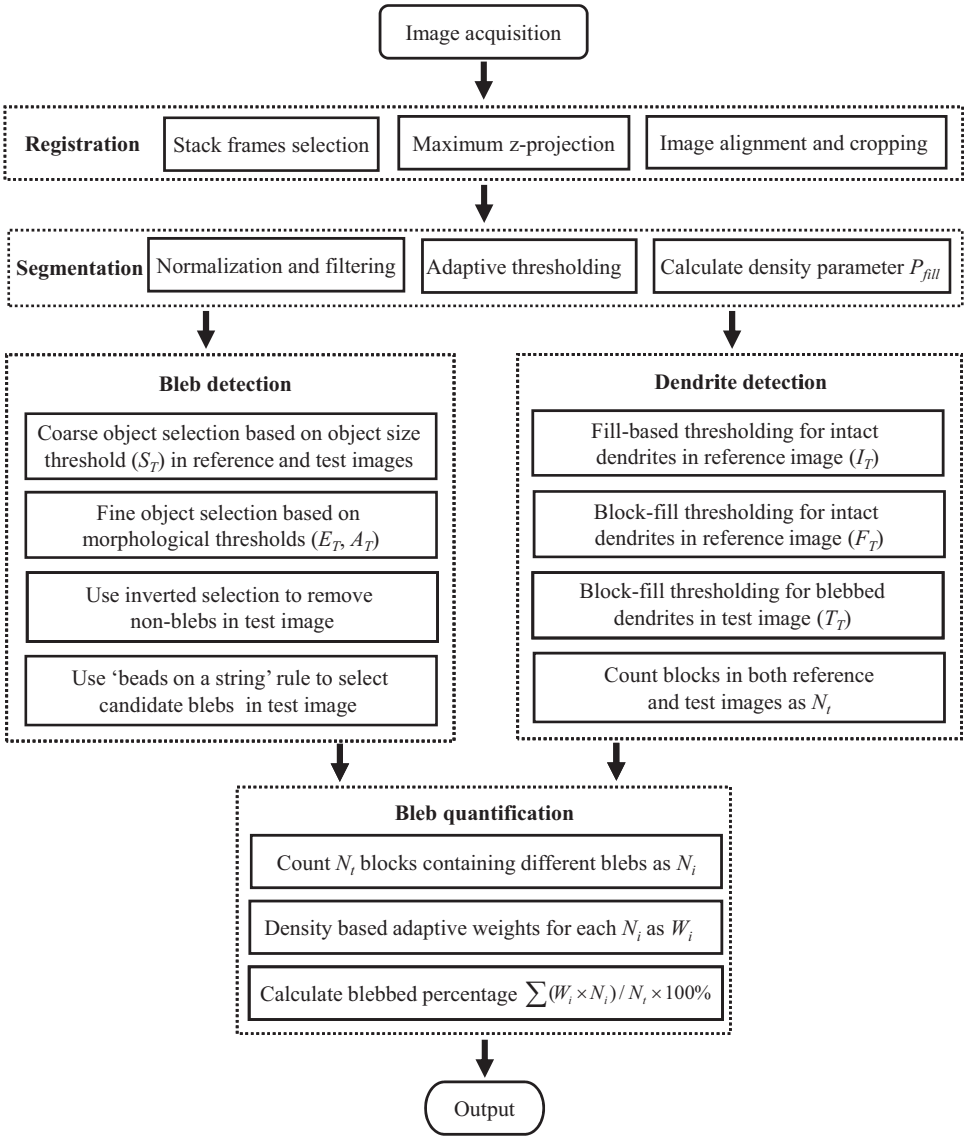

Fig. 1. Flowchart of steps in automated analysis of blebbed dendrites.

study. Transgenic mice were bred at the University of British Columbia animal facilities. All the animal preparations (anesthesia, surgery and physiological maintenance) were similar to previous reports (Murphy et al., 2008). Briefly, anesthesia was induced with intraperitoneal injection of urethane (0.12% w/w) and body temperature was maintained at $37 \pm 0.5\,^{\circ}$C using a heating pad and feedback regulation from a rectal temperature probe. The 5 datasets used in this study were chosen since they contained a wide-range of dendritic blebbing values and were from experiments where the brain temperature was regulated to $32\,^{\circ}$C. These conditions were similar to the brain surface temperature in previous work where a craniotomy with a coverslip was used (Murphy et al., 2008). For a comparison to data obtained at $37\,^{\circ}$C see Liu and Murphy (2009). A cranial window over the right somatosensory cortex for *in vivo* 2P imaging was performed. A model of global ischemia, described in detail previously (Murphy et al., 2008), consisting of bilateral occlusion of the common carotid arteries was used to induce strokes. Images were acquired by custom software (Igor) and using an Olympus (Tokyo, Japan) IR-LUMPlanFl water immersion objective [40×, 0.8 numerical aperture (NA)]. 2P imaging using an excitation wavelength of 900 nm was performed to obtain 3D image stacks with 1 μm z-resolution before and during ischemia and less frequently following reperfusion to avoid potential laser damage. Most images of dendrites were taken within the first 70 μm of cortex where the dendrites of layer V neurons project laterally within layer I. The images were acquired with a pixel width of 0.2 μm and a pixel area of 0.04 μm^2, spanning an area of $205 \times 205\ \mu m^2$ (i.e., 1024×1024 pixels). In this paper, when referring to distances within images, unless noted otherwise, distances will be given in pixels.

The experimental protocols were approved by the University of British Columbia animal care committee and consistent with Canadian Council on Animal Care and Use guidelines.

2.2. Manual image analysis

Manual analysis of images was performed using tools in ImageJ software (http://rsb.info.nih.gov/ij/). Prior to analysis, maximal intensity z-projections of 3D image stacks were aligned using the translation function from the ImageJ *StackReg* plugin (Thevenaz et al., 1998) and cropped with ImageJ geometric operations. To assess the extent of dendritic blebbing with global ischemia, we determined the percentage of blebbed dendrites in acquired 3D image stacks and maximal intensity z-projections. Analysis of den-

drite structure was aided by the use of a grid with 20 μm blocks (i.e., 100 pixels) placed in ImageJ (Li and Murphy, 2008; Murphy et al., 2008). Only blocks containing visible dendrites were considered for manual analysis and dendritic segments would be scored as either blebbed or intact. We used the same criteria for manually scoring dendrites as blebbed as in previous reports, where blebbing is distinguished as exhibiting round or ellipsoid structures regularly separated by regions of little or no fluorescence (Murphy et al., 2008). Dendritic blebs were distinguished from spherical axonal boutons and dendrites cut in cross section by examining 3D stacks and making comparisons to pre-ischemic conditions (Murphy et al., 2008).

2.3. Image registration

For the purposes of this paper, when referring to the steps involved in developing the automated approach, the reference image refers to the pre-ischemia image and test images are all images acquired during ischemia and reperfusion which are compared with the reference image.

Image registration corrects for translational movement of the imaging tissue which can occur over the time course of imaging and/or as a result of stroke and reperfusion. Here, we first took maximal intensity z-projections of 3D image stacks (20 sections × 1 μm) acquired pre-ischemia, during ischemia and reperfusion, generating 2D images (Fig. 2(a)). We avoided the projection of corrupted frames (occurring as a result of turning on and off PMTs during image acquisition or large translational shifts occurring during ischemia and reperfusion), by employing a frame selection method based on correlation analysis of successive frames where only successive and highly correlated frames were selected for z-projection. From our datasets, we found that most projection images contained all 20 frames within a stack. Following image z-projection, a subpixel image registration algorithm using the MATLAB function *dftregistration* (Guizar-Sicairos et al., 2008) was applied (Fig. 2(b)). Images were then cropped using 100 × 100 pixels blocks for subsequent steps in image analysis.

2.4. Image processing and thresholding

For image thresholding, it is necessary to convert the 2P-acquired 16-bit grayscale image, I, to an image matrix of normalized intensities, I_N, between [0,1] with double precision as following:

$$I_N = \frac{I - I_{min}}{I_{max} - I_{min}} \quad (1)$$

where I_{min} and I_{max} are the minimum and maximum intensity levels, respectively. A median filter (radius = 1 pixel) was applied to images to reduce photon and PMT noise generated from 2P imaging, and the resulting image was named I_{NF}.

Otsu's thresholding method was applied to convert the grayscale image to a binary image generating a global threshold, O_T. This method allows the extraction of dendrites from the background by automatically segmenting an image into two classes of pixels. Pixels are classed as either background or foreground (in this case, the foreground being dendrites) by selecting the optimal threshold, O_T (in the grayscale image) which maximizes the separability of the classes (Otsu, 1979). The MATLAB function *graythresh* searched for the O_T that minimizes the intra-class variance, defined as a weighted sum of variances of the two classes:

$$\min_{O_T}(\omega_1(O_T)\delta_1^2(O_T) + \omega_2(O_T)\delta_2^2(O_T)) \quad (2)$$

where weights, ω_i, are the probabilities of the two classes separated by O_T, and δ_i^2, are the variances of these classes. A reference image was converted with this way to a binary image, I_R.

Inspired by Cheng et al.'s (2007) work, an adaptive local threshold was defined for robust segmentation of blebs from inhomogeneous background or lower intensity regions within an image. For both reference and test images, I_{NF}, a mean smooth filtering was executed in I_{NF} with 10 × 10 pixels size sliding window to obtain I_{SF}. In I_{SF}, the mean intensity value of the first 10 brightest blocks was calculated as M_B. The local threshold, T_L, is defined as the following:

$$T_L = O_T \times (2 \times (M_B/O_T) \times I_{SF} + 1 - 2 \times M_B) \quad (3)$$

Here, the local threshold, T_L, is a 2D matrix of the same size as image I_{NF}. From this, the binary image I_B can be derived as:

$$I_B = \begin{cases} 1, & \text{if } I_{NF} > T_L \\ 0, & \text{else} \end{cases} \quad (4)$$

Using this method, pixels belonging to dendrites were marked as '1' and background as '0'. Representative binary images of dendrites pre-ischemia, during ischemia, and in reperfusion following the local thresholding method are shown in Fig. 2(c).

2.5. Morphology analysis

Based on previous reports (Hasbani et al., 2001; Kirov et al., 2004; Li and Murphy, 2008; Murphy et al., 2008; Obeidat et al., 2000; Park et al., 1996; Risher et al., 2010; Zhang et al., 2005; Zhang and Murphy, 2007), a coarse size threshold, S_T, was set to identify all objects in I_B to be blebs if they had a diameter between 0.5 and 5 μm (i.e., 2.5–25 pixels in diameter and area of 6.25–625 pixels) such that:

$$6 < S_T < 625 \quad (5)$$

We considered four parameters to further characterize objects meeting the threshold set in Eq. (5): *Eccentricity*, *Centroid*, *Area* and *Solidity*. *Eccentricity* (values ranging from 0 to 1) describes circularity where 0 denotes an object which is a perfect circle and 1 denotes a line. *Centroid* defines the *x* and *y* coordinates of an object by referring to its center of mass. *Area* defines size, calculated from the total pixels making up an object. *Solidity* describes the shape and is computed as *Area*/*ConvexArea*, where *ConvexArea* is the smallest convex polygon area that can contain the object.

Objects in I_B were then identified using the MATLAB function *bwlabel* where all connected pixels of an object were labeled with an integer to form a label matrix, I_L, with positive integer elements corresponding to different objects (Haralick and Shapiro, 1992). For example, all pixels labeled '0' make up the background, '1' make up one object, '2' make up a second object, and so forth. The MATLAB function *regionprops* then returned measurements on *Eccentricity*, *Centroid*, *Area* and *Solidity* of the labeled objects (blob analysis). By examining the distribution of *Eccentricity* and *Area* (Fig. 3), thresholds for eccentricity, E_T, and area, A_T, were used for fine detection of candidate blebs in reference and test images as follows:

$$E_T < 0.9 \quad (6)$$

$$\begin{cases} A_T > 40 \\ A_T < 4 \times \text{mean}(A) \end{cases} \quad (7)$$

Here, an eccentricity of 0.9 indicates the ratio of the semi-minor and semi-major axes of an ellipse to be 0.45. Mean(A) is the averaged area of all the objects satisfying Eq. (5). Table 1 gives values from one experiment for objects meeting criteria defined in Eqs. (5)–(7).

Fig. 4 shows key steps in coarse to fine bleb detection by applying Eqs. (5)–(7). To avoid mislabeling objects as blebs, we assumed that all objects satisfying Eqs. (6) and (7) in the reference image were not blebs, but were instead axonal boutons, spines, and cross

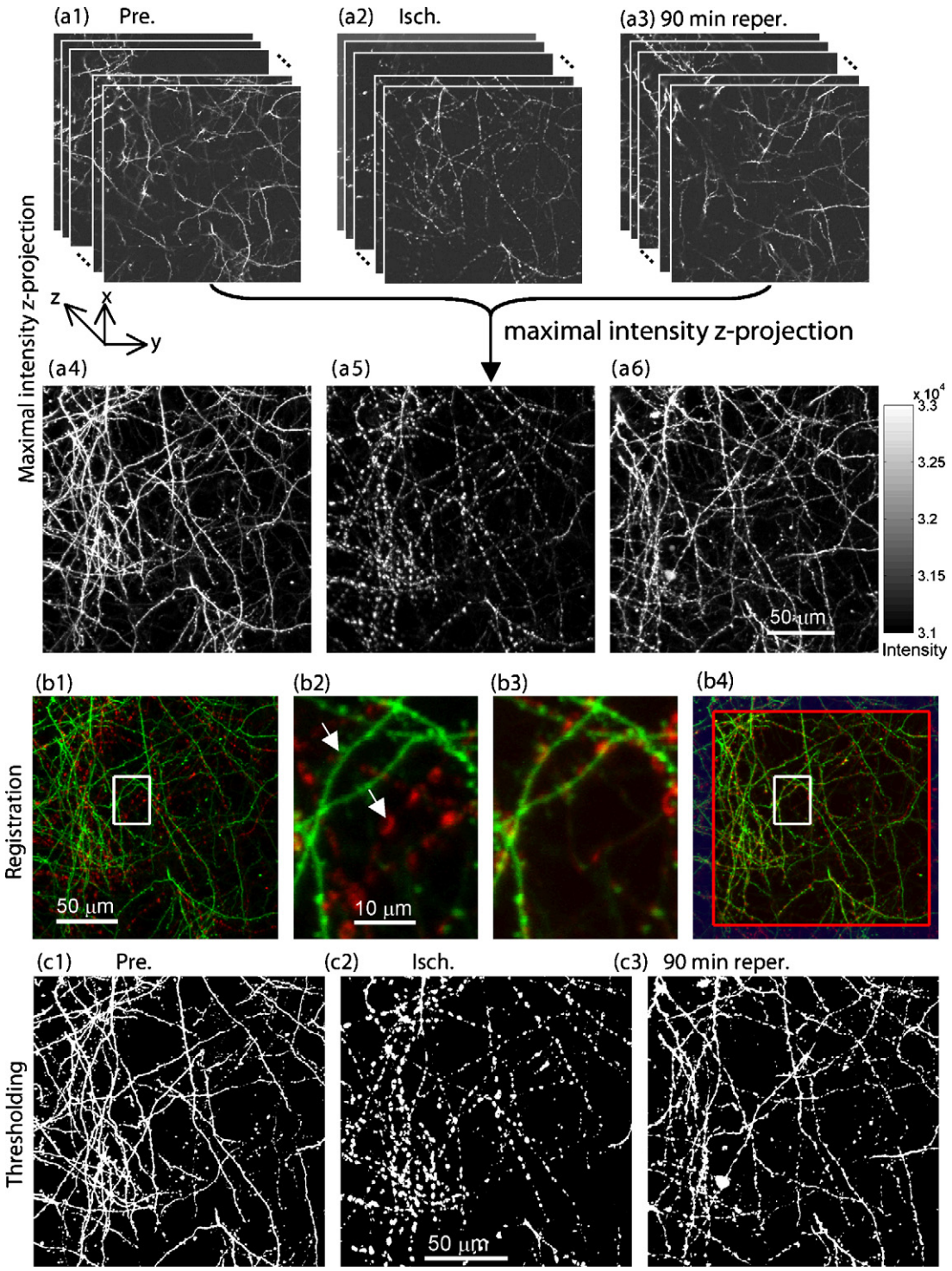

Fig. 2. Initial image processing steps involved in this study. Maximal intensity z-projections of 16-bit 3D image stacks to produce 2D images (a1–a6). 3D image stacks acquired pre-ischemia (a1), during ischemia (a2), 90 min after reperfusion (a3) with corresponding 2D maximal intensity z-projections (a4–a6). Each 3D image stack has 20 frames, 1 μm/frame. Scale bar is 50 μm in (a4–a6). Example of image registration for the alignment of 2P images acquired pre- and during ischemia (b1–b4): unregistered merged pre-ischemia (green) and ischemia (red) 2P images (b1). An enlarged view (b2) of the area outlined in (b1) shows images acquired pre and during ischemia are not aligned (white arrows show the location of the same dendritic branch in pre-ischemia and ischemia images), but translational shifts are corrected following application of the MATLAB function *dftregistration* (b3). (b4) shows registered merged pre-ischemia and ischemia images. The area (900 × 900 pixels) bound by the red box is cropped for further image analysis. Scale bar is 50 μm for (b1 and b4) and 10 μm for (b2 and b3). Binary images pre-ischemia (c1), during ischemia (c2), and after 90 min of reperfusion (c3) following application of local thresholding method. All the images are cropped to 900 × 900 pixels. Scale bar is 50 μm.

sections of dendrites, and thus for automated analysis, the percentage of blebbed dendrites in pre-ischemia images is defaulted to 0%. These objects were used to form an inverted selection mask for test images. A *Solidity* threshold (<0.7) was also set to remove the mislabeling of hollow or irregular objects as candidate blebs in test images. The identified number of candidate blebs after fine detection in both reference and test images were recorded as N_{Ref} and N_{Test}. These values were used for bleb quantification.

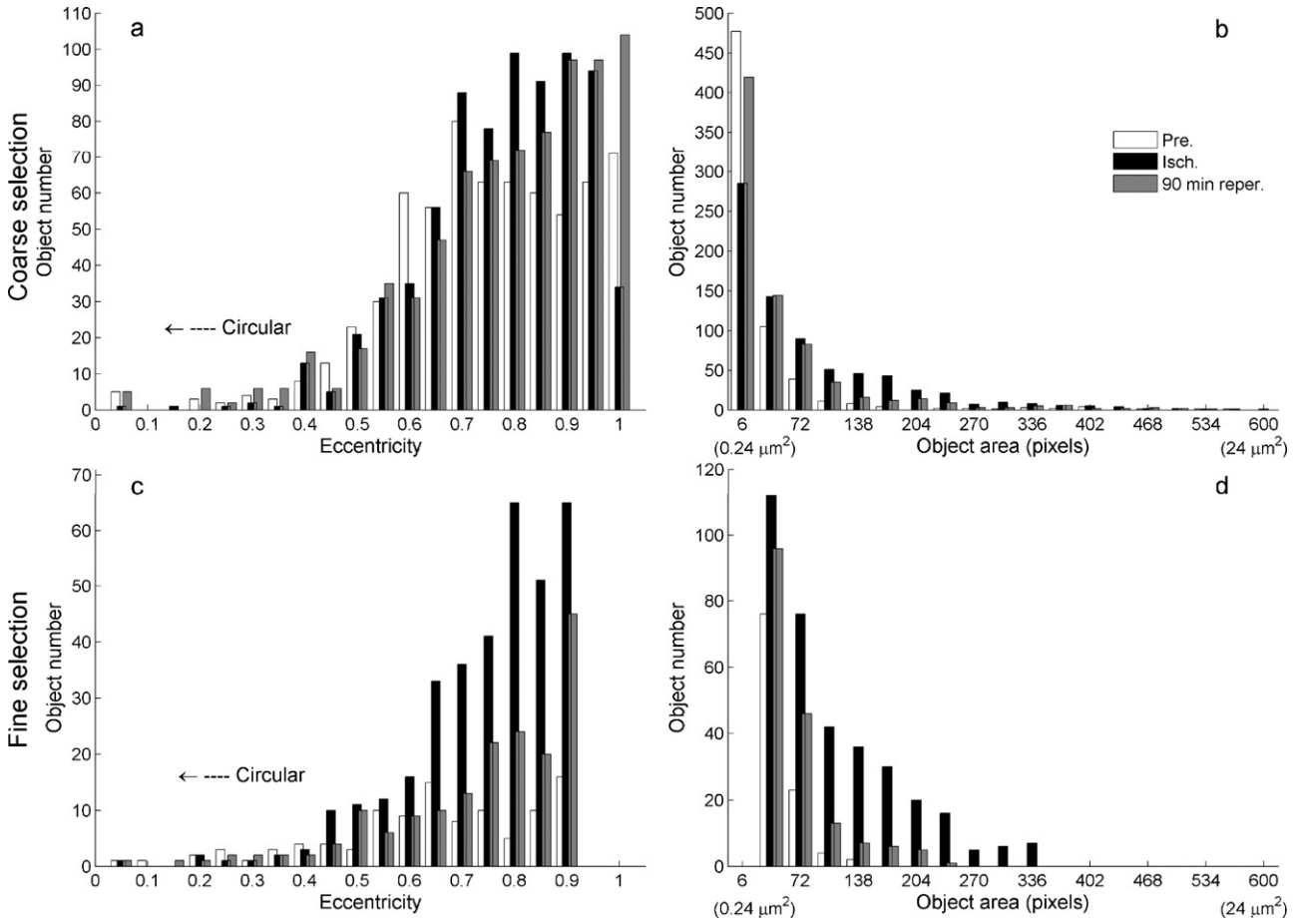

Fig. 3. Histograms showing distribution of object eccentricity and area (in pixels) after coarse selection according to $6 < S_T < 625$ (a and b) and fine selection according to $E_T < 0.9$ and $40 < A_T < 4 \times \text{mean}(A)$ (c and d). Values are shown for pre-ischemia (white bars), ischemia (black bars), and after 90 min of reperfusion (gray bars). The arrow in (a and c) refers to lower eccentricity values and more circular objects. The values in brackets (b and d) indicate the pixel to μm conversion (area of 1 pixel = 0.04 μm²).

2.6. Dendrite detection and bleb quantification

Within a 100×100 pixels grid, we selected for blocks in the binary reference image, I_B, containing clear and intact dendrites by applying adaptive threshold method based on the density of GFP or YFP labeled dendrites. Here, the filling probability (P_{fill}) was calculated as:

$$P_{fill} = \frac{\text{sum}(I_R)}{D_x \times D_y} \quad (8)$$

where sum (I_R) is the total number of dendrites labeled as '1' from the Otsu's thresholding method and D_x and D_y denote pixels on the x- and y-axis, respectively. To ensure that structures in I_B were correctly identified as dendrites and analyzed dendrites were contained within blocks, two additional thresholds based on the density of labeled dendrites were defined. The intact dendrite threshold, I_T, sets the minimum area (in pixels) required to be considered a dendrite, and the block-fill threshold, F_T, describes the minimum pixels from dendrite structure which must be contained within a single block. These thresholds are defined below:

$$I_T = 200 + 0.6 \times P_{fill} \times (100 \times 100) \quad (9)$$

$$F_T = 0.5 \times I_T \quad (10)$$

Table 1
Example morphological parameters from an experiment.

	Pre-ischemia	Ischemia	90 min Reper.
Number of coarsely selected objects	661	750	759
Morphological parameters			
Eccentricity, $\bar{E}$ (mean ± SD)	0.72 ± 0.18	0.75 ± 0.15	0.76 ± 0.19
Area, $\bar{A}$ (mean ± SD)			
Pixels	42.1 ± 64.6	94.4 ± 98.6	63.7 ± 82.5
μm²	1.68 ± 2.58	3.78 ± 3.94	2.55 ± 3.00
Morphological thresholds			
Eccentricity threshold, E_T	0.9	0.9	0.9
Area threshold, A_T			
Pixels	40–168.4	40–377.6	40–254.8
μm²	1.60–6.74	1.60–15.1	1.60–10.2
Number of objects after fine selection	105	350	174

Through coarse selection, all objects meeting $6 < S_T < 625$ pixels (Eq. (5)) are detected in pre-ischemia, ischemia, and reperfusion images. Mean values for *Eccentricity* $\bar{E}$ and *Area* $\bar{A}$ for these objects are given as mean ± SD. By further satisfying morphological thresholds, thresholds of *Eccentricity* E_T and *Area* A_T, as defined in Eqs. (6) and (7), objects undergo a fine selection process to detect candidate blebs.

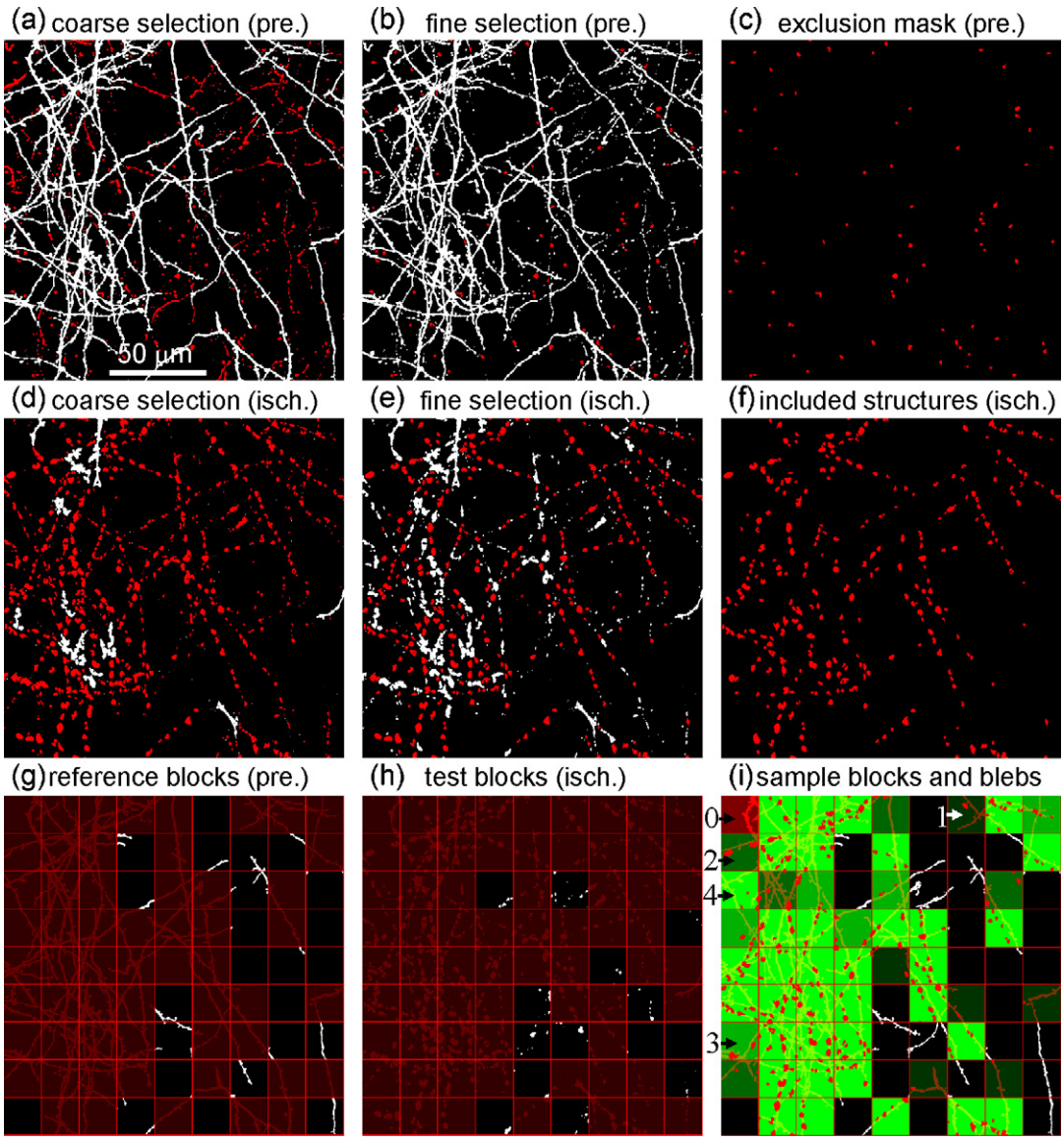

Fig. 4. Key steps in automated analysis of blebbed dendrites. Selected coarse objects (red) meeting the criteria set by $6 < S_T < 625$ (a) and fine object selection based on meeting $E_T < 0.9$ and $40 < A_T < 4 \times \text{mean}(A)$ thresholds (b) in pre-ischemia (reference) images. Objects selected through coarse (d) and fine (e) selection in ischemic (test) images. Red marked objects in (c) satisfying $6 < S_T < 625$ in the reference binary image which are non-blebs (spines, axonal boutons, and dendrites in cross section). (c) is used as an exclusion mask derived from (b) to perform inverted selection in (e) leaving included structures (candidate blebs) in (f). (g) Red blocks (reference blocks) in reference image of intact dendrites fulfill I_T and F_T. (h) Red blocks (test blocks) in test image fulfill $0.5 \times F_T$. (i) Only blocks present in both the reference (g) and test image (h) (candidate blocks) are selected for bleb quantification. The number of these blocks is recorded as N_t. The level of green shading relates to the scaled number of blebs contained within the block (1, 2, 3, or ≥4), with examples shown with number and arrow. The shaded red blocks contain intact dendrite segments with no blebs. In this example, the percentage of blebbed dendrites was calculated to be 93.1% with Eq. (13).

For analysis, dendrites must have a minimum area of I_T and occupy blocks with pixels larger than the F_T threshold. In the reference image, blocks meeting these criteria were taken as reference blocks (Fig. 4(g)). Because interbleb regions have little or no fluorescence, test blocks in test images were selected if the threshold, T_T, met:

$$T_T > 0.5 \times F_T \tag{11}$$

An additional condition was applied such that foreground pixels number in test blocks was at least one quarter of the pixels number of intact dendrites in corresponding reference blocks (see example in Fig. 4(h)). Only blocks in both reference and test images, termed candidate blocks, were considered for bleb quantification (Fig. 4(i)). The total number of candidate blocks was recorded as N_t.

Since blebs are derived from a pre-ischemia parent dendrite, a criterion was applied that candidate blebs must be aligned with intact dendrites in the reference binary image. For this, the *Centroid* coordinates of blebs were required to be located along intact dendrites in the reference image. However, because the MATLAB *dftregistration* function only corrects for *x*- and *y*-translation, blebs in test images may not be fully aligned with the parent dendrite in the reference image if warping of brain tissue occurs following stroke and/or reperfusion. To account for warping, we allow an about 30 pixels radius of tolerance between blebs and parent dendrite by applying an about 30 pixels image dilation of the reference binary image. The dilated image was then used as a mask to select for fitted blebs for inclusion in bleb quantification. We scaled the number of blebs in each N_t block into four levels containing 1, 2, 3, or ≥4 blebs (example shown in Fig. 4(i)). Blocks were defined

based on the scaled number of blebs as $N_i (i = 1, 2, 3, 4)$ and assigned adaptive weights W_i as the following:

$$W_i = \begin{cases} \min\left(1, \dfrac{0.02}{P_{\text{fill}}} \times \dfrac{N_{\text{Test}}/N_{\text{Ref}}}{N_{\text{Ref}}/N_t}\right), & i = 1 \\ \min\left(1, \dfrac{0.08}{P_{\text{fill}}} \times \dfrac{N_{\text{Test}}/N_{\text{Ref}}}{N_{\text{Ref}}/N_t}\right), & i = 2 \\ \min\left(1, \dfrac{0.24}{P_{\text{fill}}} \times \dfrac{N_{\text{Test}}/N_{\text{Ref}}}{N_{\text{Ref}}/N_t}\right), & i = 3 \\ \min\left(1, \dfrac{0.60}{P_{\text{fill}}} \times \dfrac{N_{\text{Test}}/N_{\text{Ref}}}{N_{\text{Ref}}/N_t}\right), & i = 4 \end{cases} \quad (12)$$

The percentage of blocks containing blebbed dendrites, P_b, was then defined as:

$$P_b = \sum_{i=1}^{4} \frac{W_i \times N_i}{N_t} \times 100\% \quad (13)$$

In cases where there was less than a 5% difference between N_{Ref} and N_{Test} or if N_{Test} was smaller than N_{Ref} by at most 4 blebs, we took a new P_b as:

$$P_b = \begin{cases} 0.05 \times P_b, & \text{if } N_{\text{Test}} < 1.05 \times N_{\text{Ref}} \text{ or } N_{\text{Test}} < N_{\text{Ref}} + 4 \\ P_b, & \text{else} \end{cases} \quad (14)$$

2.7. Graphical user interface

Based on the approach discussed herein, we designated *BlebQuant* as a MATLAB graphical user interface for performing automated analysis of blebbed dendrites (Supplementary Fig. 1). This toolkit program can work under 3 different modes and for all cases the user is required to select 2P-acquired 3D image stacks for automated analysis. Mode 1 allows the user to perform step-by-step image processing and analysis by selecting the following operations: 'LoadRef'/'LoadTest' for loading images, 'PlayRef'/'PlayTest' for viewing 3D image stacks, 'ProjRef'/'ProjTest' to z-project 3D image stacks, 'PreRegist' to view alignment of images, 'Register' for aligning images, 'ThreshRef'/'ThreshTest' to convert from the grayscale (8–16 bit) to binary image, and 'Calculate' to determine bleb morphology values and blebbing percentage. Mode 2 executes the aforementioned operations for all image files within an experiment folder once the user selects reference and test images. Mode 3 performs batch processing for several experiments once pathways for folders are provided in an excel file. Bleb quantification results are written to an excel file.

3. Results

3.1. Morphological features of ischemia

The experimental results presented here are from a model of global ischemia (Murphy et al., 2008). In both manual and automated approaches, we identified dendrites as blebbed if they exhibited regularly spaced and rounded herniations that were punctuated by inter-bleb regions with lower, or in some cases nearly undetectable fluorescence (Murphy et al., 2008). If bleb identification relied solely on meeting the coarse selection size threshold of $6 < S_T < 625$, many detected objects have small areas (<40 pixels) and eccentricities near 1 that are inconsistent with typical blebs (Fig. 3(a and b)). We verified by visual inspection that these objects were not blebs, but instead were spines, axonal boutons, dendrites, or noise (Fig. 4(a and d)). To improve the accuracy of the automated approach, both E_T and A_T were used to identify candidate blebs. Table 1 gives the number of objects that meet the respective coarse and fine selection thresholds for pre-ischemia, 661/105, during ischemia, 750/350, and after 90 min of reperfusion, 759/174.

Fig. 3 shows results from one experiment illustrating eccentricity and area distributions for objects meeting the coarse (a and b) and fine (c and d) selection thresholds. A greater number of objects during ischemia met the eccentricity (<0.9) and area ($40 < A_T < 4 \times \text{mean}(A)$) thresholds to be defined as a bleb. Compared to ischemia, there is a greater number of objects with an eccentricity >0.9 in images acquired pre-ischemia and after 90 min of reperfusion (Fig. 3(a)), indicating the presence of relatively intact dendrites as seen in Fig. 2(c3).

The mean correlation, r, between the manual and automated methods for determination of blebbed dendrite percentages was 0.92 ($p < 0.01$) (Fig. 5(a)). When we applied this algorithm to chart blebbing onset and recovery in 5 animals, no significant difference was found between the manual and automated methods of blebbing quantification (by two-way ANOVA, $p = 0.86$) (Fig. 5(b)).

3.2. Applicability to different datasets

GFP and YFP expressing transgenic mice show different labeling densities in layer 5 neurons. Fig. 6 shows examples of reference images from 3 experiments where the labeling density assessed by P_{fill} (Eq. (8)) ranged from 0.04 (low density) to 0.35 (high density). As shown in Fig. 6(d), low and medium densely labeled specimens ($P_{\text{fill}} < 0.2$) show high correlation (>0.9) between manual and automated methods of analysis, but the correlation for a high density specimen was reduced to 0.77.

In comparing the same datasets converted from 16 to 8 bit images, the correlation for blebbing quantification for the different bit depths had a correlation coefficient of 0.99.

4. Discussion

We have provided an automated approach to perform analysis of dendritic blebbing as a result of ischemia. Previously, reports have described various algorithms for identification and quantification of spines (Cheng et al., 2007; Koh et al., 2002; Yuan et al., 2009; Zhang et al., 2007, 2010). Here, we add to the study of dendrite structure by describing an approach for evaluating ischemia-induced dendritic blebbing.

Under fluorescence microscopy, blebbed dendrites are distinguished from normal dendrites by the appearance of localized spherical and/or ellipsoid regions separated by inter-bleb regions of little or no fluorescence (Hasbani et al., 2001; Li and Murphy, 2008; Murphy et al., 2008; Obeidat et al., 2000; Park et al., 1996; Zhang et al., 2005; Zhang and Murphy, 2007). In previous work, a 5-point rating scale was used to reflect dendritic damage qualitatively (Zhang and Murphy, 2007). While this procedure is rapid and simple, it does not provide a quantitative assessment of dendritic damage. Recently, we have scored dendritic segments to calculate the percentage of blebbed dendrites in individual imaging stacks (Li and Murphy, 2008; Murphy et al., 2008), however manual assessment of blebbed dendrites is time-consuming and observer dependent.

With the automated method, we can quickly perform analysis on experimental datasets to determine morphological parameters, bleb location, and the percentage of blebbed dendrites for one 20-frame image stack within 60 s (using an Intel(R) Pentium(R) D CPU 2.80 GHz processor; RAM, 2038 MB). For the discussed algorithm, the use of adaptive thresholds (O_T, L_T, A_T, I_T, F_T, T_T) allow for automatic thresholding and blocks selection based on image properties of each dataset (Table 2). In particular, we feel adaptive image thresholding using T_L for segmenting dendrites from the

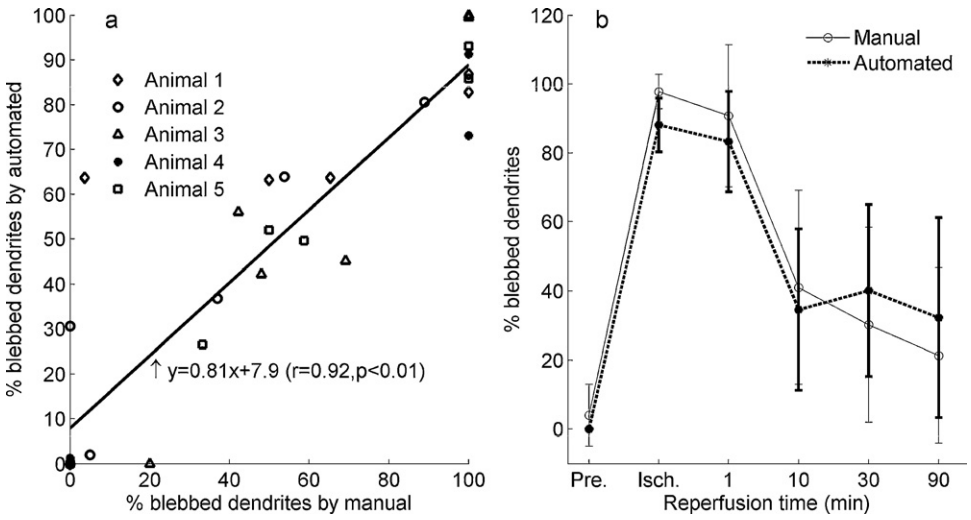

Fig. 5. (a) Correlation between automated and manual methods of analyses. (b) Percentage of blebbed dendrites pre-ischemia, during ischemia, and at indicated time points during reperfusion as determined by automated and manual analyses. No significant difference is found between the two methods (by two-way ANOVA, $p = 0.86$).

background is a critical feature for analysis since it takes into consideration changes in image signal to noise ratio that can occur with ischemia. For example, both YFP and GFP fluorescent proteins are pH sensitive such that a 1-unit change in pH during ischemia (Back et al., 2000) can result in a 50% reduction in fluorescence (Griesbeck et al., 2001; Llopis et al., 1998). Because of this, it is conceivable that alterations in pH could affect image quality and the outcome of the various image processing routines we employ. A_T allows for variation in bleb size, and I_T, F_T and T_T take into consideration dendrite density that can vary between experiments. Constant parameters (such as the factors in Eqs. (3), (7), (9)–(12) and (14)) that are used in this study were determined by fitting sample datasets that were used for optimization only. These values were then applied to 5 test datasets from different animals shown in Fig. 5. In this study we have used 100×100 pixels blocks ($400\ \mu m^2$) since they contain a reasonable number of dendrites for bleb analysis. However, the block size can be changed to match the sampling parameters used, or to provide an additional level of precision.

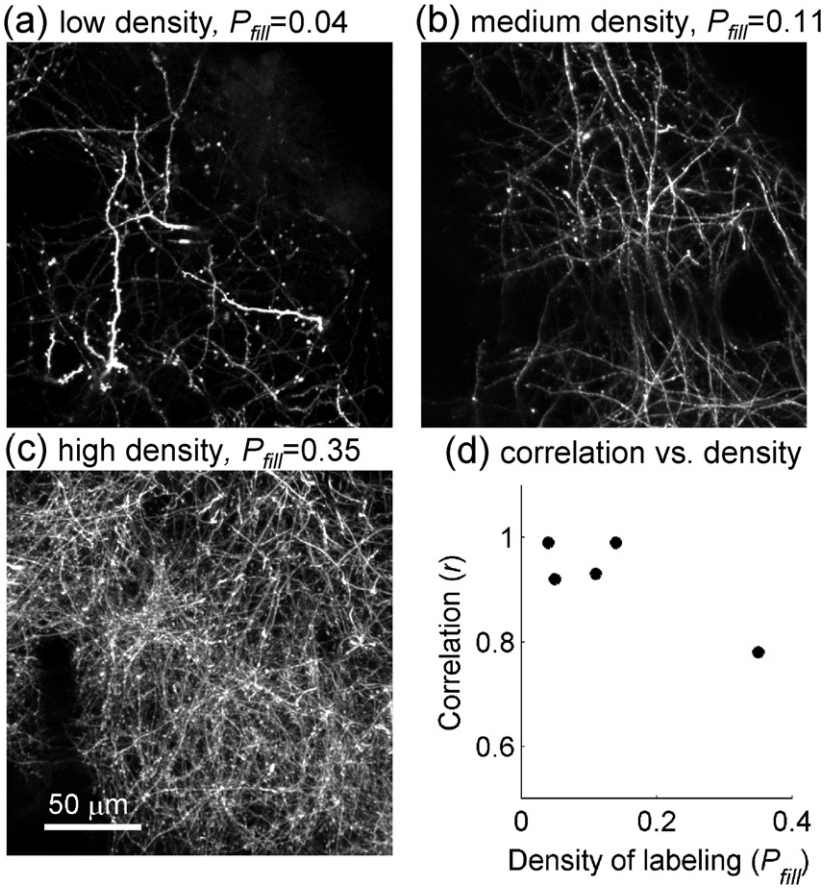

Fig. 6. Example reference images from specimens expressing low, medium, and high density of GFP labeling (a–c). (d) Correlation between manual and automated methods of analysis for different P_{fill} values.

Table 2
Description of thresholds used in *BlebQuant* algorithm.

Name	Equation	Description
O_T[a]	$\min_{O_T}(\omega_1(O_T)\delta_1^2(O_T) + \omega_2(O_T)\delta_2^2(O_T))$	Otsu's thresholding method for image segmentation
L_T[a]	$T_L = O_T \times (2 \times (M_B/O_T) \times I_{SF} + 1 - 2 \times M_B)$	Adaptive local thresholding method
S_T	$6 < S_T < 625$	Coarse object selection based on size
E_T	$E_T < 0.9$	Fine object selection based on shape
A_T[a]	$40 < A_T < 4 \times \text{mean}(A)$	Fine object selection based on size
I_T[a]	$I_T = 200 + 0.6 \times P_{fill} \times 100 \times 100$	Intact dendrite threshold for block selection in reference image
F_T[a]	$F_T = 0.5 \times I_T$	Block-fill threshold for block selection in reference image
T_T[a]	$T_T = 0.5 \times F_T$	Block-fill threshold for block selection in test image

[a] Adaptive thresholds.

We acknowledge limitations of the current approach to aid further development of the automated method. Firstly, we have performed analysis on 2D maximal intensity projections from 10 to 20 μm of cortex. 3D analysis of image stacks has been used recently for spine and bouton detection (De Paola et al., 2006; Yuan et al., 2009; Zhang et al., 2010) and in future work, quantification of dendritic blebbing could be extended to 3D stacks. Secondly, the translational registration method employed in this work is not optimal for datasets where tissue warping occurs following ischemia, and future improvement of this toolkit program can employ a non-rigid registration method. Thirdly, the current method sets the blebbing percentage of the reference image to be 0% and as such the program provides relative changes in blebbing with respect to a pre-ischemia condition. Due to the fact that other round objects may be detected as blebs (such as axonal boutons or dendrites in cross section), we feel this simplification is required to facilitate the detection and quantification of blebs. The program can be improved to independently identify blebs and quantify damage irrespective of a reference image.

In summary, we provide a new tool for automated analysis of dendritic structural alterations that result from ischemia. While we demonstrate the use of this toolkit in a model of global ischemia, we anticipate future applications of our automated analysis include the examination of blebbing in focal models of ischemia (Li and Murphy, 2008; Zhang et al., 2005), and in apical and basal dendritic processes in relation to distances to an ischemic core within single neurons (Brown et al., 2008), and to assess blebbing during ischemic and non-ischemic events such as cortical spreading depression (Takano et al., 2007) and peri-infarct depolarizations (Risher et al., 2010). While we apply this algorithm for analyzing blebbed dendrites in stroke, it is also applicable for the study of structural alterations in a wide variety of neurological disorders (Kuchibhotla et al., 2008).

Information sharing statement

The *BlebQuant* toolkit package and some of the image stacks for validation are available online from http://www.neuroscience.ubc.ca/faculty/murphy_software.

Acknowledgments

The authors would like to thank Pumin Wang and Cindy Jiang for assistance with surgical preparations and Alexander Goroshkov and Jamie Boyd for technical assistance. This work was supported by a Heart and Stroke Foundation of BC and Yukon grant in aid to THM, in part by a CIHR operating grant (MOP49586) to THM, and an NSERC studentship to ST.

Appendix A. Supplementary data

Supplementary data associated with this article can be found, in the online version, at doi:10.1016/j.jneumeth.2010.12.018.

References

Back T, Hoehn M, Mies G, Busch E, Schmitz B, Kohno K, et al. Penumbral tissue alkalosis in focal cerebral ischemia: relationship to energy metabolism, blood flow, and steady potential. Ann Neurol 2000;47:485–92.
Brown CE, Li P, Boyd JD, Delaney KR, Murphy TH. Extensive turnover of dendritic spines and vascular remodeling in cortical tissues recovering from stroke. J Neurosci 2007;27:4101–9.
Brown CE, Murphy TH. Livin' on the edge: imaging dendritic spine turnover in the peri-infarct zone during ischemic stroke and recovery. Neuroscientist 2008;14:139–46.
Brown CE, Wong C, Murphy TH. Rapid morphologic plasticity of peri-infarct dendritic spines after focal ischemic stroke. Stroke 2008;39:1286–91.
Cheng J, Zhou X, Miller E, Witt RM, Zhu J, Sabatini BL, et al. A novel computational approach for automatic dendrite spines detection in two-photon laser scan microscopy. J Neurosci Methods 2007;165:122–34.
Davalos D, Grutzendler J, Yang G, Kim JV, Zuo Y, Jung S, et al. ATP mediates rapid microglial response to local brain injury in vivo. Nat Neurosci 2005;8:752–8.
De Paola V, Holtmaat A, Knott G, Song S, Wilbrecht L, Caroni P, et al. Cell type-specific structural plasticity of axonal branches and boutons in the adult neocortex. Neuron 2006;49:861–75.
Feng GP, Mellor RH, Bernstein M, Keller-Peck C, Nguyen QT, Wallace M, et al. Imaging neuronal subsets in transgenic mice expressing multiple spectral variants of GFP. Neuron 2000;28:41–51.
Griesbeck O, Baird GS, Campbell RE, Zacharias DA, Tsien RY. Reducing the environmental sensitivity of yellow fluorescent protein. Mechanism and applications. J Biol Chem 2001;276:29188–94.
Guizar-Sicairos M, Thurman ST, Fienup JR. Efficient subpixel image registration algorithms. Opt Lett 2008;33:156–8.
Haralick RM, Shapiro LG. Computer and Robot Vision. Boston: Addison-Wesley; 1992.
Hasbani MJ, Schlief ML, Fisher DA, Goldberg MP. Dendritic spines lost during glutamate receptor activation reemerge at original sites of synaptic contact. J Neurosci 2001;21:2393–403.
Kirov SA, Petrak LJ, Fiala JC, Harris KM. Dendritic spines disappear with chilling but proliferate excessively upon rewarming of mature hippocampus. Neurosci 2004;127:69–80.
Koh IY, Lindquist WB, Zito K, Nimchinsky EA, Svoboda K. An image analysis algorithm for dendritic spines. Neural Comput 2002;14:1283–310.
Kuchibhotla KV, Goldman ST, Lattarulo CR, Wu HY, Hyman BT, Bacskai BJ. Aβ plaques lead to aberrant regulation of calcium homeostasis in vivo resulting in structural and functional disruption of neuronal networks. Neuron 2008;59:214–25.
Li P, Murphy TH. Two-photon imaging during prolonged middle cerebral artery occlusion in mice reveals recovery of dendritic structure after reperfusion. J Neurosci 2008;28:11970–9.
Liu RR, Murphy TH. Reversible cyclosporin A-sensitive mitochondrial depolarization occurs within minutes of stroke onset in mouse somatosensory cortex in vivo, a two-photon imaging study. J Biol Chem 2009;284:36109–17.
Llopis J, McCaffery JM, Miyawaki A, Farquhar MG, Tsien RY. Measurement of cytosolic, mitochondrial, and Golgi pH in single living cells with green fluorescent proteins. Proc Natl Acad Sci U S A 1998;95:6803–8.
Mostany R, Chowdhury TG, Johnston DG, Portonovo SA, Carmichael ST, Portera-Cailliau C. Local hemodynamics dictate long-term dendritic plasticity in peri-infarct cortex. J Neurosci 2010;30:14116–26.
Murphy TH, Li P, Betts K, Liu R. Two-photon imaging of stroke onset in vivo reveals that NMDA-receptor independent ischemic depolarization is the major cause of rapid reversible damage to dendrites and spines. J Neurosci 2008;28:1756–72.
Obeidat AS, Jarvis CR, Andrew RD. Glutamate does not mediate acute neuronal damage after spreading depression induced by O_2/glucose deprivation in the hippocampal slice. J Cereb Blood Flow Metab 2000;20:412–22.

Otsu N. A threshold selection method from gray-level histograms. IEEE Trans Syst Man Cybern 1979;9:62–6.
Park JS, Bateman MC, Goldberg MP. Rapid alterations in dendrite morphology during sublethal hypoxia or glutamate receptor activation. Neurobiol Dis 1996;3:215–27.
Risher WC, Ard D, Yuan J, Kirov SA. Recurrent spontaneous spreading depolarizations facilitate acute dendritic injury in the ischemic penumbra. J Neurosci 2010;30:9859–68.
Spires TL, Meyer-Luehmann M, Stern EA, McLean PJ, Skoch J, Nguyen PT, et al. Dendritic spine abnormalities in amyloid precursor protein transgenic mice demonstrated by gene transfer and intravital multiphoton microscopy. J Neurosci 2005;25:7278–87.
Takano T, Tian GF, Peng W, Lou N, Lovatt D, Hansen AJ, et al. Cortical spreading depression causes and coincides with tissue hypoxia. Nat Neurosci 2007;10:754–62.
Thevenaz P, Ruttimann UE, Unser M. A pyramid approach to subpixel registration based on intensity. IEEE Trans Image Process 1998;7:27–41.
Yuan X, Trachtenberg JT, Potter SM, Roysam B. MDL constrained 3-D grayscale skeletonization algorithm for automated extraction of dendrites and spines from fluorescence confocal images. Neuroinformatics 2009;7:213–32.
Zhang SX, Boyd J, Delaney K, Murphy TH. Rapid reversible changes in dendritic spine structure in vivo gated by the degree of ischemia. J Neurosci 2005;25:5333–8.
Zhang SX, Murphy TH. Imaging the impact of cortical microcirculation on synaptic structure and sensory-evoked hemodynamic responses in vivo. PLoS Biol 2007;5:1152–67.
Zhang Y, Chen K, Baron M, Teylan MA, Kim Y, Song Z, et al. A neurocomputational method for fully automated 3D dendritic spine detection and segmentation of medium-sized spiny neurons. Neuroimage 2010;50:1472–84.
Zhang Y, Zhou X, Witt RM, Sabatini BL, Adjeroh D, Wong ST. Dendritic spine detection using curvilinear structure detector and LDA classifier. Neuroimage 2007;36:346–60.